Integrin Binding Immunoglobulin Type Filamin Domains Have Variable Stability[†]

Pengju Jiang and Iain D. Campbell*

Biochemistry Department, University of Oxford, Oxford OX1 3QU, U.K.

Received June 19, 2008; Revised Manuscript Received September 1, 2008

ABSTRACT: Filamin, a large modular protein composed mainly of many immunoglobulin-like domains, is a potent cross-linker of actin filaments. The region containing immunoglobulin type modules 19−21 makes up the binding site for the cytoplasmic tails of the integrin adhesion receptors. Here we investigate the stability of the Ig-like filamin domains using NMR studies over a range of pH and temperature. We show that the 21st Ig-like module (FLNa21) is partly unfolded even under physiological conditions and when attached to FLNa20. It is, however, appreciably stabilized upon binding to integrins. FLNa21 is noticeably less stable than neighboring homologous modules, such as FLNa19 and FLNa17. This variability in stability could be related to the known sensitivity of filamin to cell-mediated mechanical forces.

Filamin, first identified as "actin binding protein" (*1, 2*), is widely expressed in animal cells. It is essential for fetal development and cell locomotion (*3*), and mutations in filamin genes result in various malformation diseases (*4*−*6*). This potent actin filament cross-linker is a large homodimeric modular protein (*3*). In addition to an actin binding domain consisting of two calponin homology modules at the N-terminus, all filamins are composed of a number of homologous domains (90−100 residues) that dimerize at the C-terminal domain. Human filamin has 24 immunoglobulin-like modules (IgFLMN)[1] that can be identified by domain identification tools (*7*). Here we will call these domains FLNa1−FLNa24. Filamins use some of these modules to associate directly with the cytoplasmic tails of transmembrane proteins, including integrins (*8*), tissue specific human platelet factor CD-42 (*9*), and T-cell CD-4 (*10*) and CD-28 (*11*). Although the total number of modules varies, depending on the source, filamins generally form rather extended structures (*12*). Their extended conformation and ability to cross-link cytoskeleton and plasma membrane proteins make filamins plausible contributors to the delivery of cellular forces (*13*). The IgFLMN modules have relatively poor sequence conservation, even within the same species; for example, only one proline residue is strictly conserved in the 24 aligned modules from human filamin isoform A.

In the past decade, tens of human filamin ligand proteins, including many signaling proteins, have been identified (*3, 5, 12*). Most ligands preferentially bind to the FLNa15−24 region (*12*), and FLNa21 and FLNa19 were found to contain integrin binding sites in pull-down assays (*14*). While investigating filamin binding to integrins using NMR (*14, 15*), we observed quite distinct stabilities among the FLNa modules that are further tuned by ligand association. These observations are the subject of this paper.

MATERIALS AND METHODS

Sample Preparation. The preparation and NMR assignment for [U-^{15}N]FLNa21 WT, C2293S (amino acids 2236−2329, GenBank accession number P21333), FLNa19 (amino acids 2045−2141), FLNa17 (amino acids 1863−1956), FLNa20 (amino acids 2141−2235), and FLNa19−21 (amino acids 2045−2329) have been reported previously (*9, 14, 15*). The domain boundaries are predicted to cover the structural regions validated by previous crystallography and NMR work (*9, 14, 15*). The purity of the proteins was checked by SDS−polyacrylamide gel electrophoresis, size-exclusion chromatography, and electrospray ionization mass spectroscopy. The integrin β7-derived peptide, ^{776}PLYKSAITTTINP^{788} (N-terminally acetylated and C-terminally amidated), was purchased from EZBiolab.

Collection of NMR Spectra and Data Processing. All NMR samples were buffered with 50 mM sodium phosphate (pH 6.10) containing 100 mM NaCl, 5 mM dithiothreitol (only for proteins with cysteine), and 0.02% sodium azide in 90% H_2O and 10% D_2O. The NMR sample temperature was calibrated using methanol chemical shifts (*16*).

A water-flip-back gradient-enhanced heteronuclear single-quantum correlation spectroscopy (HSQC) pulse sequence was used for protein characterization and protein−ligand studies (*17*). The relative peak intensities were found to be relatively insensitive to variable relaxation times, as long as the recycle time was longer than 1.5 s; HSQC spectra, collected using ^{1}H frequencies of 500 and 600 MHz and relaxation delays of 2 s, were used to measure peak volumes. The NMR characterization of backbone dynamics, which included heteronuclear NOE, T_1, and T_2 measurements, was carried out using previously described pulse sequences (*18*). The heteronuclear NOE effects were calculated as the ratios between the peak heights in the spectra recorded with and without ^{1}H saturation during the 3 s recycle delay.

[†] This work was supported by grants from BBSRC (BB/F006845/1) and the Wellcome Trust. P.J. acknowledges support from the Clarendon Fund and an Overseas Research Student Award scheme during his D.Phil. studies.

* To whom correspondence should be addressed. Telephone: +44 1865 275346. Fax: +44 1865 275253. E-mail: iain.campbell@bioch.ox.ac.uk.

[1] Abbreviations: IgFLMN, filamin type immunoglobulin domain; FLNa, human filamin isoform A; HSQC, heteronuclear single-quantum correlation spectroscopy.

10.1021/bi8011466 CCC: $40.75
Published on Web 09/26/2008

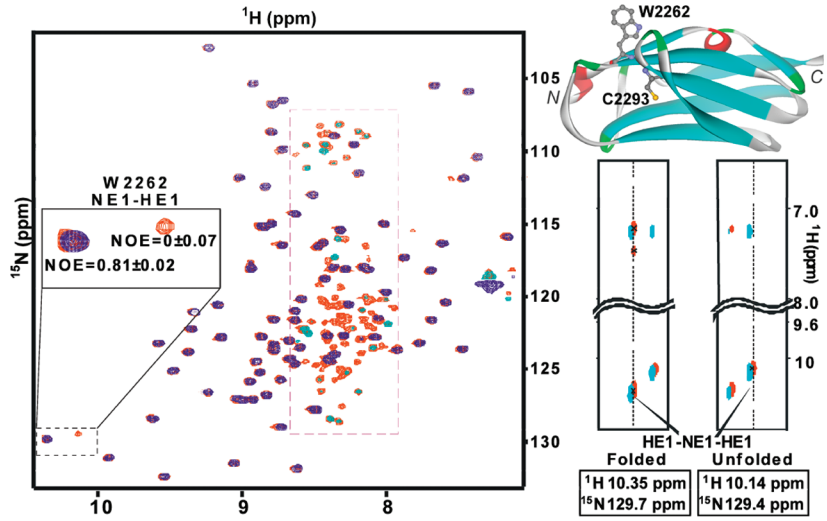

FIGURE 1: Folding equilibria observed under normal NMR experimental conditions. ^{1}H−^{15}N HSQC spectra with the heteronuclear NOE applied [NOE "on" spectrum (+, blue; −, cyan) on top of the NOE "off" spectrum (+, red; −, green)] show that the FLNa21 C2293S mutant contains flexible regions corresponding to a partially unfolded fraction under mild conditions (pH 6.10 and 25 °C). Among the unfolded peak set, an isolated peak pair (shown in the extracted inset of the spectral window) could be assigned to the side chain NH group of the unique tryptophan residue (W2262 NE1−HE1) as suggested by the similar TOCSY (cyan layer) and NOESY (red layer) strips. This side chain is located on the surface of the folded protein, as revealed by the crystal structure (the side chains of W2262 as well as C2293 are shown on a ribbon diagram of FLNa21, from PDB entry 2BRQ). All the NMR spectra were recorded on a 600 MHz machine.

All spectra were referenced to water [$\delta(H_{water}) = 4.766 - 0.0119 \times (T - 25)$ ppm, where T is the temperature in degrees Celsius (*19*)] with indirect referencing in the nitrogen dimension [^{15}N−^{1}H frequency ratio = 0.101329118 (IUPAC)]. NMR data processing was carried out with NMRPipe (*20*) and Sparky (www.cgl.ucsf.edu/home/sparky). For peak volume integration, the direct dimension and the indirect dimension were zero-filled to 5K and 1K points, respectively; the window functions in both dimensions were replaced with an exponential function which does not change the integral intensities (*21*). Integration was conducted using Lorentzian 2D peak shape fitting, and the peak volume errors were derived by calculating the fitting residues as described in Sparky.

Thermal Folding Stability Analysis. Only two states could be detected in slow exchange, so the folding equilibria were assumed to involve a two-state folding−unfolding transition. The side chain NH group of tryptophan is well-resolved from other NH peaks in HSQC spectra [typically $\delta(W_{HE1}) > 10$], and the peak position was different for the folded and unfolded species. Therefore, this isolated signal was used as a quantitative measure of the fraction folded. The side chain of the FLNa W2262 residue points outward to the solvent in the folded state, when both free and bound to integrin tails (*14*). The similarity of solution environments of the two peaks is confirmed by the observation that the shift in fluorescence maximum ($\lambda^{\varepsilon}_{max}$) is less than 2 nm and the temperature coefficients of the side chain NH group of both folded and unfolded states are the same (−5 ppb/°C). As a result, it is possible to employ the integrated volumes of the NH peaks to calculate the folded (f) and unfolded (f_u) fraction of total protein, provided that a sufficiently long recycle time is applied between successive transients:

$$f = 1 - f_u = I_f/(I_f + I_u) \quad (1)$$

where I_f is the folded peak volume and I_u the unfolded peak volume. This method of quantification was not used when FLNa20 was attached because the tryptophan then became partially buried (*15*).

The folding equilibrium constant (K_u) and free energy difference (ΔG) of the unfolding transition can be derived from the equation

$$\Delta G = -RT \ln K_u = -RT \ln[f_u/(1 - f_u)] \quad (2)$$

where R is the gas constant and T the temperature in kelvin. The resulting Gibbs free energy difference at constant temperature is (*22*)

$$\Delta G = \Delta H_m(1 - T/T_m) + \Delta C_p[T - T_m - T \ln(T/T_m)] \quad (3)$$

where T_m is the transition temperature (melting point), ΔH_m the transition enthalpy at the corresponding T_m, and ΔC_p the heat capacity change upon transition. According to the derivation principle of this equation, the fitting for folding data against temperature is that of a parabola, so one folding data set can be fitted to two pairs of solutions for T_m and ΔH_m with an identical ΔC_p; the two solutions describe the two transitions separately. Data fitting was carried out using Origin.

Assuming the protein is fully bound, the ligand can be regarded as part of the complex and the same thermal equations can be applied to folding equilibria of the complex (^{unfolded}FLNa21 + ^{unbound}ITβ7 ↔ ^{folded}FLNa21−ITβ7). Assuming the unfolded protein cannot bind ligand, the folding equilibrium curves for the free protein and complex should merge at high temperatures. This prediction is consistent with the observed folding curve of the FLNa21 C2293S mutant in the presence of the integrin β7 peptide (Figure 3A).

RESULTS

FLNa21 Experiences Unfolding Equilibria under Physiological Conditions. The majority of the FLNa21 NMR spectra could be characterized and assigned and the integrin binding site mapped (*14*). However, tens of weak peaks (red peaks in the spectrum in Figure 1) were always observable,

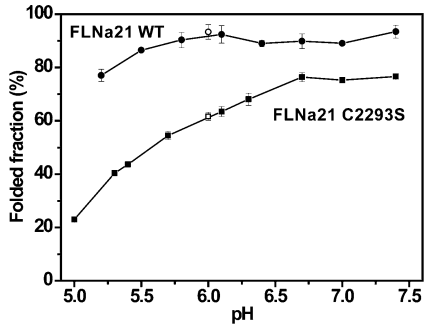

FIGURE 2: Acid-induced denaturation of FLNa21. The pH-dependent unfolding curves show turning points around pH 6 for both the wild type (●) and C2293S mutant (■) of FLNa21. The unfolded fractions after low-pH and high-pH cycles (from pH 2 to 10) are denoted with white symbols; the match suggests that the folding equilibria for both FLNa21 variants are fully reversible.

even after extensive purification by ion-exchange and size-exclusion chromatographic columns or using protein from different expression batches.

To prevent oxidization-induced multimerization, the single cysteine residue in FLNa21, C2293, was mutated to serine. Compared to the wild type, this mutated domain gave rise to even more intense "extra" peaks, although the folding topology, as revealed by the chemical shifts, is very similar (Supporting Information, Figure S2). Repeated pH−temperature HSQC titrations of FLNa21 C2293S revealed that the weaker peaks became stronger at low pH or high temperature (Supporting Information, Figure S1A). This secondary peak set represents a species with considerable flexibility since the peaks have zero or negative signal intensity in a ^{1}H−{^{15}N} heteronuclear NOE experiment (Figure 1). Taken together with their position in the spectrum (dark red dashed box region in Figure 1, 7.9−8.7 ppm in the ^{1}H dimension), this suggests that they arise from an unfolded, flexible protein. We show that their properties are consistent with a small population of unfolded FLNa21 in equilibrium with the folded form.

Quantification of the Reversible Folding Equilibria. Most of the extra peaks in NMR spectra were difficult to assign because of spectral overlap and lack of NOE signals, but the side chain NE1−HE1 peak of the unique tryptophan [see three-dimensional (3D) NOESY overlapping 3D TOCSY strip plots extracted in the left inset of Figure 1] is readily assigned. Each peak in this pair has distinct dynamic behavior (for example, at 500 MHz, $T_1 = 533 \pm 3$ ms, $T_2 = 144 \pm 2$ ms, and NOE $= 0.703 \pm 0.004$ for folded and $T_1 = 740 \pm 9$ ms, $T_2 = 199 \pm 9$ ms, and NOE $= -0.36 \pm 0.01$ for unfolded). In all titrations, this W2262 NE1−HE1 peak pair exhibited typical slow exchange behavior and the peak volumes could be used to quantify the unfolded/folded concentration ratio. Cross-peaks could, however, be observed between these two peaks in a NOESY type experiment (see Figure S1B of the Supporting Information); this is consistent with a reversible exchange process occurring between folded and unfolded states at a rate faster than $1/T_1$ (-2 s^{-1}). After all pH or temperature titration cycles, the folded portions reappeared (Figures 2 and 3), confirming reversibility. Intrinsic/extrinsic fluorescence and circular dichroism (CD) spectroscopy were also attempted, but differences between folded and unfolded states were insufficient to yield very convincing unfolding profiles, although the observations were consistent with the conclusions drawn from quantitative analysis of the Trp side chain NH NMR peaks [the Trp side chain is in a similar environment in both states, and the far-UV CD signal is weak and perturbed by the near-UV signal, a common problem for β-sheet proteins (*23*)].

pH Dependence of the Unfolded Form. The pH-dependent unfolding of FLNa21 WT and C2293S is shown in Figure 2. Both variants maintain a denatured fraction at all pH values with a significantly increasing fraction below pH 6. This behavior is similar to the pH-induced changes in chemical shifts of residues around the cysteine mutation site (Supporting Information, Figure S3). It is thus plausible that differences observed in the mutant arise from a slight pK_a change in an acidic group.

Temperature Dependence of the Unfolded Form. The fraction of the unfolded form at pH 6.1 is shown as a function of temperature in Figure 3. FLNa21 samples, especially the FLNa21 C2293S form, exhibit a strengthened unfolding tendency below 20 °C. The derived Gibbs free energy differences could be fitted to theoretical equations for thermal folding (fitting curves are shown as solid lines in Figure 3C,D). The transition point between heat denaturation and cold denaturation is seen to be around room temperature; this is relatively uncommon as the cold transition melting temperature is below the freezing point for most proteins (*24*). The FLNa21 protein samples have relatively narrow transition temperature ranges and low transition entropies (C2293S mutant, 4−35.5 °C, 85 kJ mol^{-1}; wild type, −7 to 46.9 °C, 169 kJ mol^{-1}) compared to other systems (*25*).

Integrin Binding Stabilizes FLNa21. We have previously shown that the cytoplasmic tail of integrin β-subunits forms a new antiparallel strand along strand C of FLNa21 (*14*). The integrin β7 peptides reduce the fraction of unfolded peaks in FLNa21, and the unfolding curves shift significantly toward higher temperatures (Figure 3A,B). Fitting these curves (see Materials and Methods) shows that the folding enthalpy for heat denaturation of the FLNa21 C2293S−ITβ7 complex is increased from 85 to 130 kJ mol^{-1}, and the corresponding temperature range between heat and cold denaturation was enlarged to −10 to 51 °C (Figure 3C). The fitted parameters for the thermal unfolding of FLNa21 are listed in Table 1.

FLNa21 Unfolding Equilibrium with FLNa20 Attached. FLNa21 was recently found to be bound to an N-terminal region of FLNa20 in both crystal and solution states, while FLNa19 had no contact with either FLNa20 or FLNa21 (*15*). Although FLNa19−21 aggregates in the NMR tube and only gives reasonable HSQC spectra over 30 °C, the unfolding of FLNa21 was also studied in the triple-module context. Because of the interaction with FLNa20, the W2262 side chain in FLNa19−21 is shifted in the folded form (at 37 °C and pH 6.10, $\delta_{HE1} = 10.19$ ppm and $\delta_{NE1} = 128.7$ ppm in FLNa19−21 and $\delta_{HE1} = 10.29$ ppm and $\delta_{NE1} = 129.7$ ppm in FLNa21) and becomes very weak, but the peak from the unfolded form could still be observed ($\delta_{HE1} = 10.09$ ppm and $\delta_{NE1} = 129.3$ ppm for both FLNa21 and FLNa19−21 at 37 °C and pH 6.10) (Supporting Information, Figure S4).

Similar Modules Have Distinct Stabilities. NMR and crystal structures show that FLNa17, FLNa19, and FLNa21 all have a very similar seven-stranded β-sheet sandwich structure (*9, 14, 15*). Our ^{1}H−{^{15}N} NOE experiments also indicate that the backbone flexibilities of all these domains

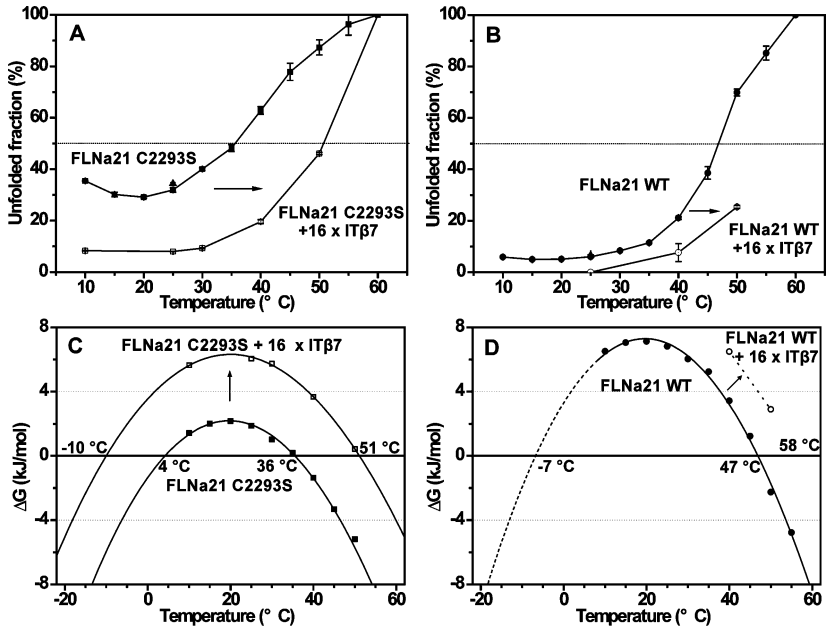

FIGURE 3: Thermal unfolding equilibria of FLNa21, and corresponding data fitting, reveal a cold denaturation contribution to unfolding and a clear stabilization effect upon ligand binding. The temperature-dependent unfolded fractions of free FLNa21 and complexes with a 16-fold excess of integrin β7-derived peptides are plotted (A) for the wild type and (B) for the C2293S mutant (black symbols for free proteins and white symbols for complexes). Repeat measurements to show reversibility are indicated with triangles. The Gibbs free energy changes (ΔG) at each titration point are derived from the unfolded fraction according to eq 2.2 and are plotted against temperature in panels C and D; the transition enthalpy change (ΔH_m) and melting temperature (T_m) for both heat denaturation and cold denaturation were fitted. The resulting parameters are listed in Table 1.

Table 1: Fitted Parameters for Thermal Folding Equilibria of FLNa21

	FLNa21 C2293S				wild type FLNa21		
	free protein		+16×ITβ7		free protein		+16×ITβ7
	heat	cold	heat	cold	heat	cold	heat
T_m (°C)	35.5 ± 0.5	4 ± 1	51.1 ± 0.2	−10 ± 1	46.9 ± 0.3	−7 ± 1	58[a]
ΔH_m (kJ mol^{-1})	85 ± 4	−79 ± 3	130 ± 3	−113 ± 3	169 ± 5	−150 ± 5	−
ΔC_p (kJ K^{-1} mol^{-1})	5.2 ± 0.3		4.0 ± 0.1		5.9 ± 0.3		−

[a] This data set was incomplete, so the temperature for heat denaturation was derived from extrapolation.

are similar (data not shown). The solution state thermal stability of these domains, however, varies significantly as shown by the effect of temperature on the HSQC spectra (Figure 4). FLNa21 is the most unstable and entirely unfolds below 60 °C. FLNa19 is fully folded even above 60 °C, whereas FLNa17 contains both folded and unfolded population at 60 °C.

FLNa20 Alone Is Partly Unfolded. FLNa20 is unable to bind integrins and exhibits unusual solution behavior. Many HSQC peaks that become apparent at increasing concentrations have much shorter T_2 relaxation times than other peaks. Heteronuclear NOE experiments also show that tens of peaks with random coil-like chemical shifts are considerably flexible (Figure 5A). These peaks could be assigned to the unfolded region of FLNa20 that zips along the C−D face of FLNa21, as discussed previously (Figure 5B) (*15*).

DISCUSSION

Some folded and unfolded peaks can be clearly separated in NMR HSQC spectra. By monitoring well-resolved resonances from tryptophan as a function of pH and temperature, FLNa21 is shown to undergo both cold and heat denaturation around room temperature. The unfolded fraction increases in the C2293S mutation. In the presence of excess integrin β7-derived peptide, both FLNa21 variants became significantly more stable, presumably because of extra hydrogen bonding and side chain contacts that are formed in the complex (*14*).

Compared to FLNa21, FLNa19 and FLNa17 are fully folded under physiological conditions. The domain volume and total solvent accessible surface area are very similar for these three IgFLMN modules so the variable stability must mainly come from differences in primary sequence. FLNa21 seems to have more hydrophobic residues on the outer surface than its homologues. In particular, the unique tryptophan is greatly exposed. The additional hydrophobic residues are not in the hydrophobic core of the folded structure, and it is probably a residue ensemble rather than a single residue that is responsible for the low stability of FLNa21.

FLNa20 has an amino acid sequence and folding properties quite different from those of FLNa17, -19, and -21. It contains an unstructured region that is responsible for zipping along FLNa21 (*15*). Such a structural pattern, where module 2I-1 zips onto module 2I, may be commonly adopted by other even-numbered modules since the solution state structures of several other even-numbered domains from human filamin isoforms B and C (coordinates deposited in

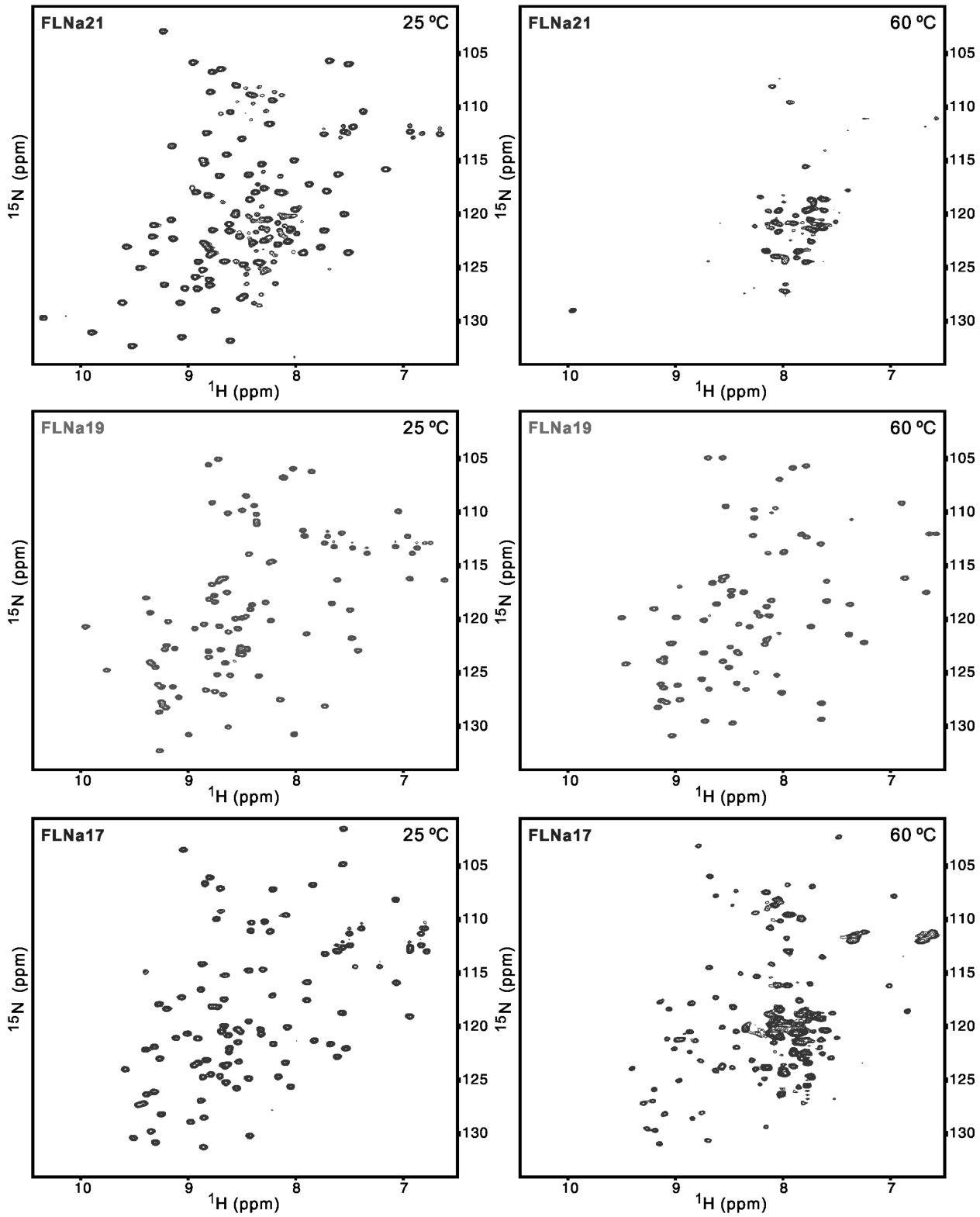

FIGURE 4: Domains with similar structure have different folding stability. The HSQC spectra of the corresponding modules [FLNa21 (top row), FLNa19 (middle row), and FLNa17 (bottom row)] at 25 (left column) and 60 °C (right column) show that FLNa21 is unfolded at 60 °C, FLNa19 is fully folded, and FLNa17 is partially unfolded. All the NMR experiments were conducted on the same 600 MHz NMR spectrometer.

Protein Data Bank by RIKEN institute) also lack a structured A strand. Although the N-terminal region of FLNa20 binds to the C−D face of FLNa21 in a manner similar to that of the tail of integrin β7, an unfolded FLNa21 fraction is still observed when FLNa is attached, possibly because the self-zipping association is much weaker than that with integrin β7 (*15*). As discussed previously (*15*), FLNa22 is not expected to stabilize FLNa21 but other types of contact from remote modules are possible although as yet unknown.

The low stability of some of these modules could have significant biological implications. For example, the intrinsic low stability of A-band Ig modules from titin is believed to be associated with the elasticity of this muscle-related protein (*26*). Unlike titin where all the Ig modules from the same

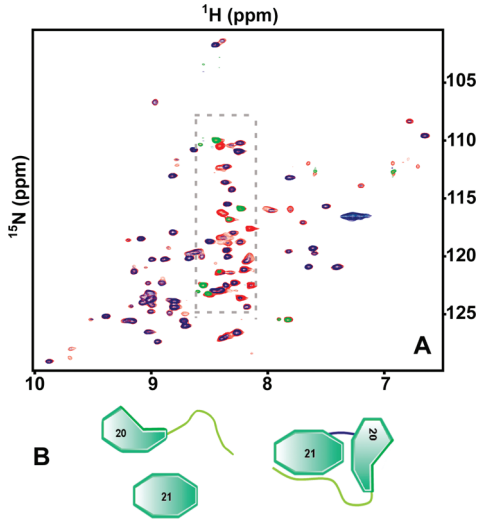

FIGURE 5: FLNa20 is partly unstructured and zips along FLNa21. (A) Overlaid spectra of FLNa20 from heteronuclear NOE experiments [NOE on spectrum (+, blue; −, green) on top of the NOE off spectrum (+, red; −, cyan)] reveal flexibility in part of the protein. Many peaks, mainly located in the middle of the HSQC spectra (the pink dashed box), have significantly reduced intensity; approximately 10 peaks showed sign inversion. Using a 1 mM protein sample, this experiment was carried out at pH 6.10 and 25 °C on a 600 MHz spectrometer. (B) Schematic illustration of partially unstructured FLNa20, fully structured FLNa21, and FLNa20 zipped along FLNa21.

functional band have a similar low stability, neighboring filamin Ig modules (FLNa17−21) have diverse stabilities even though they all bind to cell migration/adhesion proteins, such as integrins, migfilin, and glycoprotein Ibα1. An intriguing possibility is that the unusual instability of FLNa21 has been designed so that it is sensitive to a stretching-force-induced unfolding as previously reported for a homologous IgFLMN domain from amoeba, the fourth domain of *Dictyostelium discoideum* filamin; a small external stretching force can induce complete unfolding of that particular domain (*27, 28*). Preliminary atomic force microscopy (AFM) studies also showed that a 50 pN stretching force can induce unfolding of certain modules within intact human filamin A (*29, 30*). More recently, reversible unfolding of filamin modules has been suggested to act as a rheology regulator for the whole cytoskeleton network system (*31, 32*). It has also been reported that ligand binding stabilizes the stretching force resistance (*33*).

In summary, the integrin receptor region of human filamin is comprised of three successive homologous modular domains that have versatile solution behavior. FLNa19 is very stable; FLNa21 is intrinsically unstable, and FLNa20 is partly unraveled even at room temperature and neutral pH. Filamins are known to be involved in mechanical force delivery and intracellular signaling, and their IgFLMN domains exhibit distinct ligand specificity as well as stability (*3, 12*) so that various combinations of domains may be designed to be mechanical sensing devices for integrins.

ACKNOWLEDGMENT

The work began as a collaboration with Jari Ylänne (University of Jyväskylä, Jyväskylä, Finland) and David Calderwood (Yale University, New Haven, CT); they also kindly provided DNA constructs for wild type filamin fragments. We thank Dr. Jonathan Boyd and Dr. Nick Soffe for the assistance in NMR facilities as well as Dr. Christina Redfield for the help with fluorescence and circular dichroism spectroscopy measurement; Dr. Kate Wegener, Dr. Sosuke Yoshinaga, and Dr. Ioannis Vakonakis are also thanked for their assistance and their very helpful discussions.

SUPPORTING INFORMATION AVAILABLE

Figures S1−S4 showing the reversible pH and temperature titration HSQC spectra of FLNa21 C2293S, exchange cross-peaks for the two tryptophan peaks of wild type FLNa21, the chemical shift correlation for two FLNa21 variants, the pH dependence of chemical shifts from residues around the mutation site, and the unfolded peak detected for FLNa21 in the FLNa19−21 construct. This material is available free of charge via the Internet at http://pubs.acs.org.

REFERENCES

1. Hartwig, J. H., and Stossel, T. P. (1975) Isolation and properties of actin, myosin, and a new actin binding protein in rabbit alveolar macrophages. *J. Biol. Chem. 250*, 5696–5705.
2. Stossel, T. P., and Hartwig, J. H. (1975) Interactions between actin, myosin, and an actin-binding protein from rabbit alveolar macrophages. Alveolar macrophage myosin Mg^{2+}-adenosine triphosphatase requires a cofactor for activation by actin. *J. Biol. Chem. 250*, 5706–5712.
3. Stossel, T. P., Condeelis, J., Cooley, L., Hartwig, J. H., Noegel, A., Schleicher, M., and Shapiro, S. S. (2001) Filamins as integrators of cell mechanics and signalling. *Nat. Rev. 2*, 138–145.
4. Robertson, S. P. (2004) Molecular pathology of filamin A: Diverse phenotypes, many functions. *Clin. Dysmorphol. 13*, 123–131.
5. Robertson, S. P. (2005) Filamin A: Phenotypic diversity. *Curr. Opin. Genet. Dev. 15*, 301–307.
6. Robertson, S. P., Jenkins, Z. A., Morgan, T., Ades, L., Aftimos, S., Boute, O., Fiskerstrand, T., Garcia-Minaur, S., Grix, A., Green, A., Der Kaloustian, V., Lewkonia, R., McInnes, B., van Haelst, M. M., Mancini, G., Illes, T., Mortier, G., Newbury-Ecob, R., Nicholson, L., Scott, C. I., Ochman, K., Brozek, I., Shears, D. J., Superti-Furga, A., Suri, M., Whiteford, M., Wilkie, A. O., and Krakow, D. (2006) Frontometaphyseal dysplasia: Mutations in FLNA and phenotypic diversity. *Am. J. Med. Genet. 140*, 1726–1736.
7. Letunic, I., Copley, R. R., Pils, B., Pinkert, S., Schultz, J., and Bork, P. (2006) SMART 5: Domains in the context of genomes and networks. *Nucleic Acids Res. 34*, D257–D260.
8. Calderwood, D. A., Huttenlocher, A., Kiosses, W. B., Rose, D. M., Woodside, D. G., Schwartz, M. A., and Ginsberg, M. H. (2001) Increased filamin binding to β-integrin cytoplasmic domains inhibits cell migration. *Nat. Cell Biol. 3*, 1060–1068.
9. Nakamura, F., Pudas, R., Heikkinen, O., Permi, P., Kilpelainen, I., Munday, A. D., Hartwig, J. H., Stossel, T. P., and Ylanne, J. (2006) The structure of the GPIb-filamin A complex. *Blood 107*, 1925–1932.
10. Tavano, R., Contento, R. L., Baranda, S. J., Soligo, M., Tuosto, L., Manes, S., and Viola, A. (2006) CD28 interaction with filamin-A controls lipid raft accumulation at the T-cell immunological synapse. *Nat. Cell Biol. 8*, 1270–1276.
11. Thelin, W. R., Chen, Y., Gentzsch, M., Kreda, S. M., Sallee, J. L., Scarlett, C. O., Borchers, C. H., Jacobson, K., Stutts, M. J., and Milgram, S. L. (2007) Direct interaction with filamins modulates the stability and plasma membrane expression of CFTR. *J. Clin. Invest. 117*, 364–374.
12. Popowicz, G. M., Schleicher, M., Noegel, A. A., and Holak, T. A. (2006) Filamins: Promiscuous organizers of the cytoskeleton. *Trends Biochem. Sci. 31*, 411–419.
13. McGrath, J. L. (2006) Cell Mechanics: Filamin A Leads the Way. *Curr. Biol. 16*, R326–R327.
14. Kiema, T., Lad, Y., Jiang, P., Oxley, C. L., Baldassarre, M., Wegener, K. L., Campbell, I. D., Ylanne, J., and Calderwood, D. A. (2006) The molecular basis of filamin binding to integrins and competition with talin. *Mol. Cell 21*, 337–347.
15. Lad, Y., Kiema, T., Jiang, P., Pentikainen, O. T., Coles, C. H., Campbell, I. D., Calderwood, D. A., and Ylanne, J. (2007) Structure

of three tandem filamin domains reveals auto-inhibition of ligand binding. *EMBO J. 26*, 3993–4004.
16. Vangeet, A. L. (1968) Calibration of Methanol and Glycol Nuclear Magnetic Resonance Thermometers with a Static Thermistor Probe. *Anal. Chem. 40*, 2227–2229.
17. Schleucher, J., Schwendinger, M., Sattler, M., Schmidt, P., Schedletzky, O., Glaser, S. J., Sorensen, O. W., and Griesinger, C. (1994) A General Enhancement Scheme in Heteronuclear Multidimensional Nmr Employing Pulsed-Field Gradients. *J. Biomol. NMR 4*, 301–306.
18. Farrow, N. A., Muhandiram, R., Singer, A. U., Pascal, S. M., Kay, C. M., Gish, G., Shoelson, S. E., Pawson, T., Forman-Kay, J. D., and Kay, L. E. (1994) Backbone dynamics of a free and phosphopeptide-complexed Src homology 2 domain studied by ^{15}N NMR relaxation. *Biochemistry 33*, 5984–6003.
19. Wishart, D. S., Bigam, C. G., Yao, J., Abildgaard, F., Dyson, H. J., Oldfield, E., Markley, J. L., and Sykes, B. D. (1995) ^{1}H, ^{13}C and ^{15}N Chemical Shift Referencing in Biomolecular NMR. *J. Biomol. NMR 6*, 135–140.
20. Delaglio, F., Grzesiek, S., Vuister, G. W., Zhu, G., Pfeifer, J., and Bax, A. (1995) NMRPipe: A multidimensional spectral processing system based on UNIX pipes. *J. Biomol. NMR 6*, 277–293.
21. *Felix, user guide*, version 2.3 (1994) Biosym Technologies, San Diego.
22. Fersht, A. (1999) *Structure and mechanism in protein science: A guide to enzyme catalysis and protein folding*, W. H. Freeman, New York.
23. Fasman, G. D. (1996) *Circular dichroism and the conformational analysis of biomolecules*, Plenum Press, New York.
24. Kitahara, R., Okuno, A., Kato, M., Taniguchi, Y., Yokoyama, S., and Akasaka, K. (2006) Cold denaturation of ubiquitin at high pressure. *Magn. Reson. Chem. 44*, S108–S113.
25. Pastore, A., Martin, S. R., Politou, A., Kondapalli, K. C., Stemmler, T., and Temussi, P. A. (2007) Unbiased cold denaturation: Low- and high-temperature unfolding of yeast frataxin under physiological conditions. *J. Am. Chem. Soc. 129*, 5374–5375.
26. Politou, A. S., Thomas, D. J., and Pastore, A. (1995) The folding and stability of titin immunoglobulin-like modules, with implications for the mechanism of elasticity. *Biophys. J. 69*, 2601–2610.
27. Schwaiger, I., Kardinal, A., Schleicher, M., Noegel, A. A., and Rief, M. (2004) A mechanical unfolding intermediate in an actin-crosslinking protein. *Nat. Struct. Mol. Biol. 11*, 81–85.
28. Schlierf, M., and Rief, M. (2005) Temperature Softening of a Protein in Single-molecule Experiments. *J. Mol. Biol. 354*, 497–503.
29. Furuike, S., Ito, T., and Yamazaki, M. (2001) Mechanical unfolding of single filamin A (ABP-280) molecules detected by atomic force microscopy. *FEBS Lett. 498*, 72–75.
30. Yamazaki, M., Furuike, S., and Ito, T. (2002) Mechanical response of single filamin A (ABP-280) molecules and its role in the actin cytoskeleton. *J. Muscle Res. Cell Motil. 23*, 525–534.
31. DiDonna, B. A., and Levine, A. J. (2006) Filamin cross-linked semiflexible networks: Fragility under strain. *Phys. Rev. Lett. 97*, 068104.
32. DiDonna, B. A., and Levine, A. J. (2007) Unfolding cross-linkers as rheology regulators in F-actin networks. *Phys. Rev. E 75*, 041909.
33. Paci, E., and Karplus, M. (2000) Unfolding proteins by external forces and temperature: The importance of topology and energetics. *Proc. Natl. Acad. Sci. U.S.A. 97*, 6521–6526.

BI8011466